Model order reduction in unit cell modeling and its application to complex structures

R F Boukadia, C Claeys, Christophe Droz, M Ichchou, E Deckers

▶ **To cite this version:**

R F Boukadia, C Claeys, Christophe Droz, M Ichchou, E Deckers. Model order reduction in unit cell modeling and its application to complex structures. International Conference on Noise and Vibration Engineering ISMA 2018, 2018, Leuven, Belgium. pp.4663-4678. hal-03405473

HAL Id: hal-03405473
https://hal.science/hal-03405473

Submitted on 28 Oct 2021

HAL is a multi-disciplinary open access archive for the deposit and dissemination of scientific research documents, whether they are published or not. The documents may come from teaching and research institutions in France or abroad, or from public or private research centers.

L'archive ouverte pluridisciplinaire **HAL**, est destinée au dépôt et à la diffusion de documents scientifiques de niveau recherche, publiés ou non, émanant des établissements d'enseignement et de recherche français ou étrangers, des laboratoires publics ou privés.

Model order reduction in unit cell modeling and its application to complex structures

R. F. Boukadia [1,2,3], C. Claeys [1,3], C. Droz [2], M. Ichchou [2], E. Deckers [1,3]
[1] KU Leuven, Department Mechanical Engineering
Celestijnenlaan 300 B, B-3001, Heverlee, Belgium

[2] Vibroacoustics and Complex Media Group
LTDS / Ecole Centrale de Lyon,
Bat. E6, 36 Avenue Guy de Collongue, 69134 Écully, France

[3] DMMS lab, Flanders Make, Belgium

Abstract
In this work, harmonic and temporal responses of structures composed of 1D periodic waveguides are computed using the wave finite element method framework (WFEM) in conjunction with model order reduction (MOR) methods. First, a model order reduction strategy at the unit cell level is introduced and extended to parametric model order reduction (PMOR) when the mesh does not depend of the interfaces. The method relies on a mode based MOR of the inner degrees of freedom of the unit cell combined with a wave based model order reduction of the interfaces' degrees of freedom by projecting them on a collection of wave shapes obtained through the inverse approach. A first example analyses the merits of the proposed PMOR. A second example exploits the MOR method to analyze guided-waves interactions with a 3D defect in the mid-frequency domain. The proposed methodology enables the computation of highly complex and detailed models while providing substantial time reduction when computations were already possible.

1 Introduction

Wave propagation in phononic crystals and metamaterials is the center of an extensive research effort to create novel lightweight solutions with good vibroacoustic behavior. Indeed, They allow to control acoustic and elastic wave propagation thanks to a feature called band gap that correspond to frequency bands in which only spatially decaying waves can propagate. To study this new type of structures, methods based on wave propagation have been developed over the years. The Semi-Analytical Finite Element method (SAFE) [1] , the spectral finite element method [2], the shift cell operator method [3] and the WFEM [4] are some of the most popular. In particular, the last one uses classical finite element modeling of the unit cell (UC) and applies Floquet-Bloch boundary conditions a posteriori to obtain free wave propagation properties by solving a symplectic eigenvalue problem quadratic in frequency and propagation constants. The main advantages of the method are its relatively low implementation cost and the number of application cases that were developed for it [5, 6, 7, 8]. Over the years, it has proved to be a relevant method for the design and validation of both phononic crystals and resonant metamaterials [9] as well as a competitive tool for the study of coupled homogeneous and periodic waveguides. Because it rests on the resolution of an eigenvalue problem at each frequency of interest, its asymptotic complexity suffers when dealing with very large unit cells. However, classical MOR methods like Krylov subspace methods or balance truncation are not compatible with the WFEM because the spatial structure of the UC need to be preserved during the reduction process. Several methods have been developed to try and address the issue [10] [11]. This text presents some of the most recent techniques for model order reduction in unit cell modeling of 1D periodic structures and applies them to models of complex structures.

2 Unit Cell Modeling with the Wave Finite Element Method

2.1 1D WFEM: Free wave propagation

Let us consider a periodic structure composed of a unit cell (UC) that is repeated in space. To compute the wave propagation properties of such a structure the WFEM uses a finite element model of the unit cell assuming that the left and right interfaces of the UC use the same mesh and type of shape functions so that primal assembly between them is possible. The UC's degrees of freedom are then partitioned in three sub-groups. The degrees of freedom (dof) of the left interface (L), the dofs of the right interface (R) and the inner dofs (I). From there, two paths can be followed. One can chose a wavenumber and find the different frequencies and wave shapes for which such a wavenumber is relevant. This is the inverse approach. The second option is to choose a frequency and compute the properties of all propagative and decaying waves at that frequency. That is the direct approach. While the first option is generally preferred to analyze wave propagation properties over the irreducible Brillouin contours of 2D periodic structures, the second one takes precedence for most other applications. Both methods are presented below.

2.1.1 The inverse approach

The inverse approach starts with choosing a wavenumber k and thus a propagation constant $\lambda = e^{-ikL}$ where L is the length of the UC in the direction of propagation. From there, Floquet-Bloch boundary conditions can be applied to the structure and are enforced using left and right projection matrices:

$$\begin{cases} U_R = \lambda U_L \\ F_R = -\lambda F_L \end{cases} \qquad P_U(\lambda) = \begin{bmatrix} I_n & 0 \\ \lambda I_n & 0 \\ 0 & I_m \end{bmatrix} \qquad P_F(\lambda) = \begin{bmatrix} I_n & \frac{1}{\lambda} I_n & 0 \\ 0 & 0 & I_m \end{bmatrix} \tag{1}$$

Modified mass, stiffness and damping matrices are then obtained:

$$K(\lambda) = P_F(\lambda) K P_U(\lambda), \qquad M(\lambda) = P_F(\lambda) M P_U(\lambda), \qquad C(\lambda) = P_F(\lambda) C P_U(\lambda) \tag{2}$$

Finally, wave shapes and eigenfrequencies are obtained by solving the eigenvalue problem (3):

$$[K(\lambda) + i\omega C(\lambda) - \omega^2 M(\lambda)]\phi = 0 \tag{3}$$

When a real wavenumber is chosen, the modified matrices are Hermitian hence the inverse approach can be understood as a form of modal analysis. The associated eigenvalue problem has good numerical properties and optimized eigenvalue solvers have been developed to solve it.

2.1.2 The direct approach

Following the opposite path, the direct approach starts by choosing the frequency of interest and forming the dynamic stiffness matrix:

$$G = K + i\omega C - \omega^2 M \tag{4}$$

From there, the condensed dynamic stiffness matrix is obtained by condensing the internal degrees of freedom leaving only those at the interfaces as in (5):

$$D = \begin{bmatrix} D_{LL} & D_{LR} \\ D_{RL} & D_{RR} \end{bmatrix} = G_{BB} - G_{BI} G_{II}^{-1} G_{IB} \tag{5}$$

Where the index (B) corresponds to the degrees of freedom of both left and right interfaces. This operation can be costly because it requires the inversion of the matrix G_{II} at each frequency of interest. Section 3.1 shows how this can be sped up using model order reduction. Then, wave shapes ψ and propagation constants λ satisfying the Floquet-Bloch conditions (1) are looked for leading to the eigenvalue problem (6).

$$\left[\frac{1}{\lambda}D_{LR} + (D_{LL} + D_{RR}) + \lambda D_{RL}\right]\psi = 0 \tag{6}$$

This eigenvalue problem is often extremely ill-conditioned but possess a symplectic structure. However, no mainstream eigenvalue solver was developed specifically for this class of problem. The problem (6) is therefore solved as a general eigenvalue problem after being put in quadratic form. To address these issues, another equivalent form was developed by Zhong [12] . It has better numerical properties and enables the use of iterative solvers when only a few solutions are desired. It should be noted that the solutions to the eigenvalue problem come in pairs $\left(\lambda, \frac{1}{\lambda}\right)$ and (ψ^+, ψ^-) of positive and negative going waves. The MOR technique presented in section 3.2 aims at reducing the computation time of the eigenvalue problem (6).

2.2 Forced response of finite waveguides

Using solutions from the direct approach, it is possible to compute the forced response of a finite periodic waveguide composed of *N* UCs by assuming that the displacement of the *p-th* section take the form:

$$U_p = \Psi^+\Lambda^p q^+ + \Psi^-\Lambda^{N-p} q^- \tag{7}$$

Where q^+ and q^- are the amplitude coefficients for the positive and negative going waves. For free-free boundary conditions, the following formula is derived:

$$\begin{bmatrix} F_0 \\ F_N \end{bmatrix} = \begin{pmatrix} D_{LL}\Psi^+ + D_{LR}\Psi^+\Lambda & D_{LL}\Psi^-\Lambda^N + D_{LR}\Psi^-\Lambda^{N-1} \\ D_{RL}\Psi^+\Lambda^{N-1} + D_{RR}\Psi^+\Lambda^N & D_{RL}\Psi^-\Lambda + D_{RR}\Psi^- \end{pmatrix}\begin{bmatrix} q^+ \\ q^- \end{bmatrix} \tag{8}$$

Where F_0 and F_N are efforts applied at the waveguide's extremities. Another formula is used to compute the forced response of two identical periodic waveguides coupled by an arbitrary substructure. Noting D^c the condensed dynamic stiffness matrix of the substructure, a formula can be derived for the whole waveguide with free-free boundary conditions:

$$\begin{pmatrix} D_{LL}\Psi^+ + D_{LR}\Psi^+\Lambda & D_{LL}\Psi^-\Lambda^N + D_{LR}\Psi^-\Lambda^{N-1} & 0 & 0 \\ D_{RL}\Psi^+\Lambda^{N-1} + (D_{RR} + D_{LL}^c)\Psi^+\Lambda^N & D_{RL}\Psi^-\Lambda + (D_{RR} + D_{LL}^c)\Psi^- & D_{LR}^c\Psi^+ & D_{LR}^c\Psi^-\Lambda^M \\ D_{RL}^c\Psi^+\Lambda^N & D_{RL}^c\Psi^- & (D_{RR}^c + D_{LL})\Psi^+ + D_{LR}\Psi^+\Lambda & (D_{RR}^c + D_{LL})\Psi^-\Lambda^M + D_{LR}\Psi^-\Lambda^{M-1} \\ 0 & 0 & D_{RL}\Psi^+\Lambda^{M-1} + D_{RR}\Psi^+\Lambda^M & D_{RL}\Psi^-\Lambda + D_{RR}\Psi^- \end{pmatrix}\begin{bmatrix} q_1^+ \\ q_1^- \\ q_2^+ \\ q_2^- \end{bmatrix} = \begin{bmatrix} F_0 \\ 0 \\ 0 \\ F_{N+M} \end{bmatrix} \tag{9}$$

In this formula, *N* and *M* are the numbers of unit cells contained in the first and second periodic waveguides. F_0 and F_{N+M}, the efforts applied on the full structure's extremities and q_i^+ and q_i^- are the amplitude coefficients for the positive and negative going waves in each periodic waveguide.

3 Model Order Reduction Strategy

3.1 Reduction of inner degrees of freedom

To reduce the internal degrees of freedom of a UC or coupling substructure, Craig-Bamptom model order reduction [13] is used as presented in [10]. The projection matrix has two essential components. The clamped modes and the static modes of the inner degrees of freedom. The first modes are simply solution of the eigenvalue problem (10):

$$\left(K_{II} + i\omega_j C_{II} - \omega_j^2 M_{II}\right)\phi_j = 0 \tag{10}$$

Modes up to at least 3 times the maximal frequency of interest should be introduced in the projection matrix. We note those Φ_d. The static modes are given by the formula (11):

$$\Phi_s = -K_{II}^{-1}K_{IB} \tag{11}$$

The final projection matrix is :

$$P_{CB} = \begin{pmatrix} I_n & 0 \\ \Phi_s & \Phi_d \end{pmatrix} \tag{12}$$

Leading to the expression for the reduced matrices :

$$X_{red} = P_{CB}^T X P_{CB} \tag{13}$$

Where X is the original mass, stiffness or damping matrix of the model and X_{red} the reduced one.

3.2 Interface degrees of freedom reduction

3.2.1 Single Waveguide

For this case, the model order reduction scheme used is presented in [14]. It is similar to the approximations used to study acoustic wave propagation in ducts of constant cross-sections. In essence, propagative modes with cut-on frequency lower than $n_f f_m$ are used in the projection basis where n_f is a security factor usually comprised between 1 and 3 and f_m the maximal frequency of interest. When one is only interested in far field computations, n_f=1 can be used. When near field is considered a greater value may be needed. The main difference with acoustic wave propagation comes from the fact that wave propagation in solids is dispersive in wavenumber and also in mode shape (wave conversion process and veering are two extreme examples of this happening). Therefore, it is not enough to sample modes at their cut-on frequencies, rather, a sampling of the K-space using the inverse approach is realized with several wavenumber's values. A parameter n_k, an integer greater or equal to one, governs the refinement of the sampling in the wavenumber domain. In order to get a real full rank orthogonal projection matrix two operations are performed on the sampled wave modes. First, real and imaginary parts of the wave modes are separated. This addresses the issue of a complex projection matrix and lead to the creation of a vector collection ψ_{coll}. Then, a singular value decomposition (SVD) is performed on ψ_{coll} keeping only the most important left singular vectors. The exact number of vectors kept is determined by a factor $\epsilon \in \mathbb{R}_+^*$ that should generally be smaller than 10^{-3}.This leads to an orthogonal local projection matrix $Proj_{LR}$. The final projection matrix of the model is given by the block diagonal projection matrix P_{LR} :

$$P_{LR} = \begin{pmatrix} Proj_{LR} & 0 & 0 \\ 0 & Proj_{LR} & 0 \\ 0 & 0 & I_n \end{pmatrix} \tag{14}$$

Again, the reduced matrices are given by :

$$X_{red} = P_{LR}^T X P_{LR} \tag{15}$$

Where X is the original mass, stiffness or damping matrix of the model and X_{red} the reduced one.

3.2.2 Multiple waveguides and PMOR

Herein, we extend the method presented in [14] in order to build a single projection matrix valid for a family of waveguides. This allows primal assembly of reduced models when considering the coupling of different waveguides. Moreover, it can also be understood as a form of parametric model order reduction when the waveguides considered belong to a parametric family. The main interest of the method comes from the fact that reduced order models can be created on the fly at no additional computational cost which is highly beneficial when conducting phenomenological studies or optimizing parametric designs. The downsides of this approach are that an offline computation time is required to build the global projection basis and that the dofs reduction and thus the time gains are lower than those obtained using a tailored projection matrix for each model. The idea of embedding a MOR Scheme in a PMOR one is described in details in [15]. What follows shows how it is implemented in the case at hand. To create the projection matrix, one must first have a list of sample parameter values $(p_i)_{i\in[\![1,n]\!]}$. For each of these values, the reduction process is carried out as described in section 3.2.1 up to the creation of the collection of wave shapes $\psi_{coll}^{(i)}$ for the parameter

p_i. Once all wave shapes collections have been computed, they are concatenated into a single wave shape collection :

$$\Psi_{\text{coll}} = \left[\psi_{coll}^{(1)}, \psi_{coll}^{(2)}, \dots, \psi_{coll}^{(\text{n})}\right] \tag{16}$$

Again, an SVD is performed on the matrix Ψ_{coll}. Only the most prominent singular vectors are retained and used to create a local projection matrix $Proj_{LR}$ valid for the whole parametric space.

4 Numerical Examples

This section introduces two numerical examples. The first one analyses the merits and drawbacks of PMOR over MOR in a worst case scenario (for PMOR) where parameter changes lead to a localization of waves in different parts of the waveguide's cross-section. The second example highlight the power of the (MOR) strategy in enabling fast computation of wave-defect interaction in time domain for a waveguide with a high number of dofs using only the WFEM framework.

4.1 Example 1 : Parametric Model Order Reduction of a Sandwich

In this section, we study a worst case scenario for the parametric model order reduction at the interfaces' degrees of freedom by introducing an heterogeneity in the cross-section of the waveguide. This is because simply varying the material properties of an homogenous section can be understood as a shift in the maximal frequency of interest and is therefore unchallenging. The change is controlled by a parameter α which represent a scaling of the material properties. For $\alpha = 1$ the waveguide is homogeneous while the asymptotic case $\alpha = 0$ can be understood as having two decoupled waveguides. In between, strong localization phenomena in wave propagation occur due to the contrast of material properties. The nature of the parameter α makes it evident that its logarithm should be considered and therefore a lower bound strictly superior to 0 should be chosen for PMOR lest the associated part of the cross-section cannot be reduced.

4.1.1 Presentation of the model

In this section, we consider a homogeneous sandwich waveguide comprised of two materials. The material of the skins is aluminum, while that of the core is variable in both density and young modulus. The whole section is 3 centimeters wide and 5 millimeters thick with a 3 millimeters thick core and a skin thickness of 1 millimeter. A model of the cross section is created using ANSYS APDL 17 and SOLID187 elements. The mesh corresponds to a perfect grid with cubic elements of side 0.25 millimeters to ensure 4 elements in the thickness of the skins. This results in a 15246 dofs model. An illustration of the mesh is provided in Figure 1.

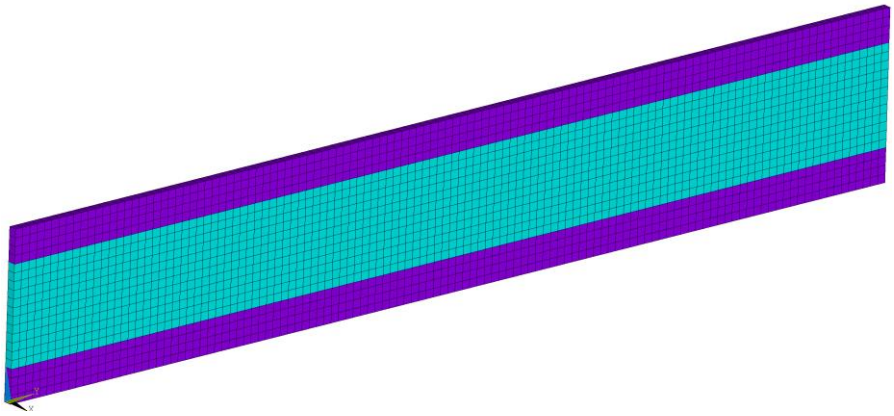

Figure 1 : Cross section of the parametric model. Material properties of the blue part are parametrized

The material properties of the skin are fixed and correspond to that of aluminum :

- Young Modulus : $E_0 = 69GPa$
- Poisson Ratio : 0.3
- Density : $d_0 = 2700\ kg.m^{-3}$
- Loss factor / hysteretic damping : $\eta = 3.10^{-3}$

The material properties of the core depend linearly on a parameter α taken in the interval $[2.10^{-1}, 1]$:

- Young Modulus : αE_0
- Poisson Ratio : 0.3
- Density : αd_0
- Loss factor / hysteretic damping : $\eta = 3.10^{-3}$

Because of this, the mass and stiffness matrices of the model can be expressed as linear combinations of 4 matrices :

$$\begin{cases} K(\alpha) = K_0 + \alpha K_1 \\ M(\alpha) = M_0 + \alpha M_1 \end{cases} \tag{17}$$

The dispersion curves obtained for extremal parameters values in the 0-60kHz frequency range are given in Figure 2. It can be observed that a low value of α accelerates the conversion of flexural waves from pure flexion to core shear. On the other hand, the compression waves and the shear wave are unaffected by the change of parameter value. This is because the mass to stiffness ratios are identical in the core and in the skins.

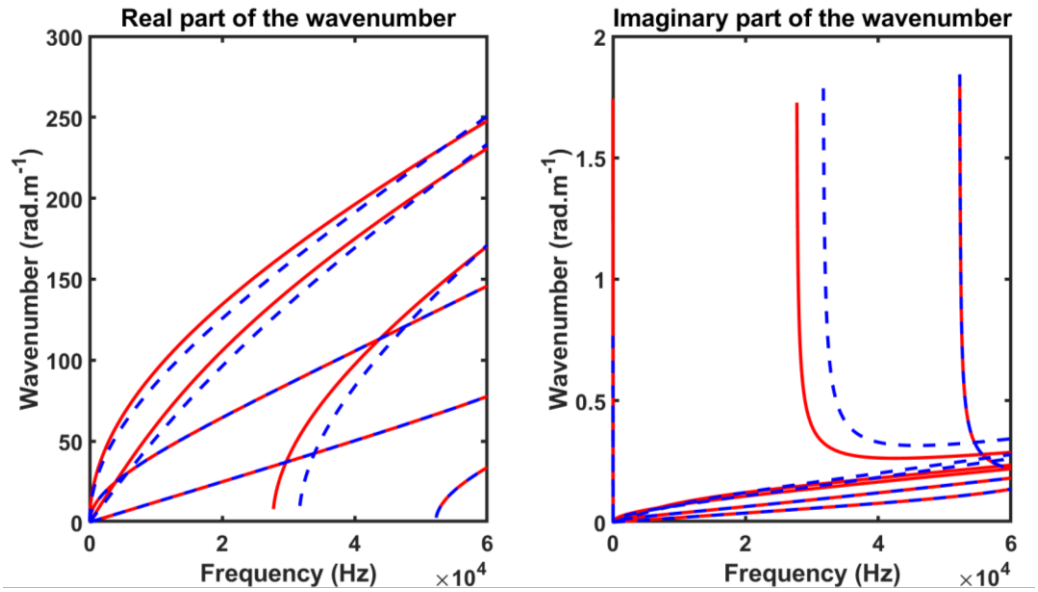

Figure 2 dispersion curves of the extremal models ($\alpha = 1$ blue ; $\alpha = 0.2$ red)

4.1.2 MOR and PMOR comparison

The MOR and PMOR strategies mostly work in the same manner with one difference. For MOR a projection basis must be created for each value of the parameter space while for PMOR a projection basis is created aggregating collections of vectors obtained at sampled values α_i. In our case, we chose a uniform logarithmic sampling for α with 10 values between 0.2 and 1. The reduced order models obtained by both strategies for a value $\alpha = 0.6003$ chosen randomly are compared in Table 1.

	MOR	PMOR
Building Reduced Model	253s	0s
Offline Computations	NA	2534s
dofs of the reduced order model	88	160
Time per eigenvalue problem	0.0094s	0.0417s

Table 1: MOR and PMOR time comparison

While creating a reduced order model using PMOR is instantaneous, there are two prices to pay for this. First, offline computations are required so that a global projection matrix can be formed. Secondly, the reduced order model obtained is bigger and therefore slower than the one obtained using MOR. Figure 3 compares the dispersion curves obtained by both methods. A perfect match is expected :

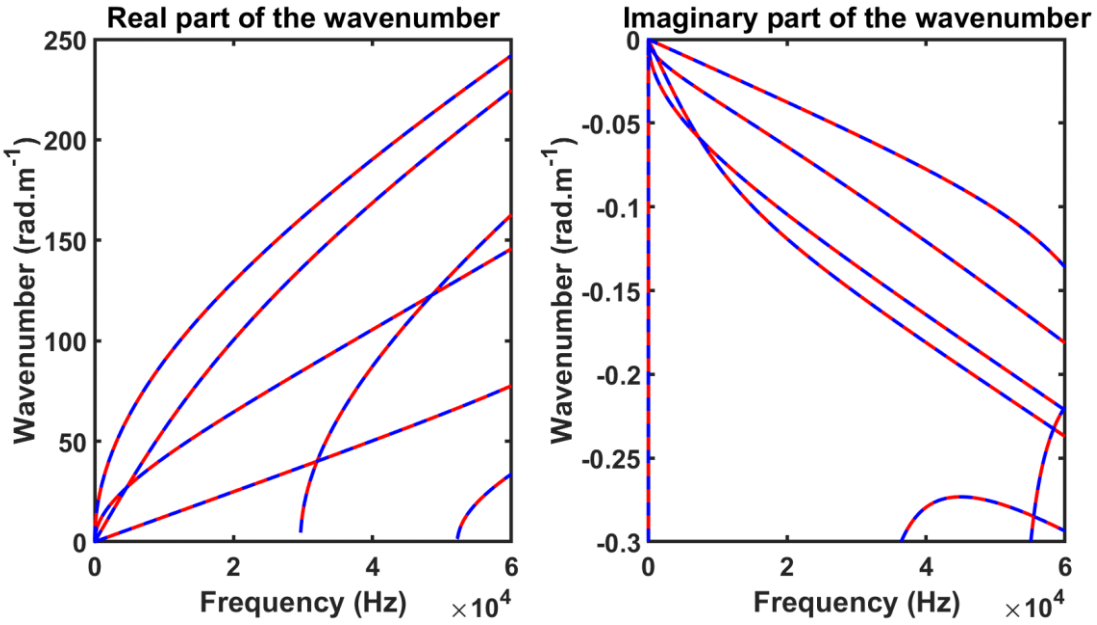

Figure 3 Dispersion curves for $\alpha = 0.6003$ MOR (red) PMOR (blue)

To complete the comparison, a forced response is computed with both models for a 40cm long waveguide with free-free boundary conditions as per the method described in section 2.2. A distributed vertical load is applied on the first section while no efforts are applied on the last one. The response is computed on the surface of the top skin on the middle of the first section ($X = 0,\ Y = 1.5\ cm,\ Z = 5\ mm$).

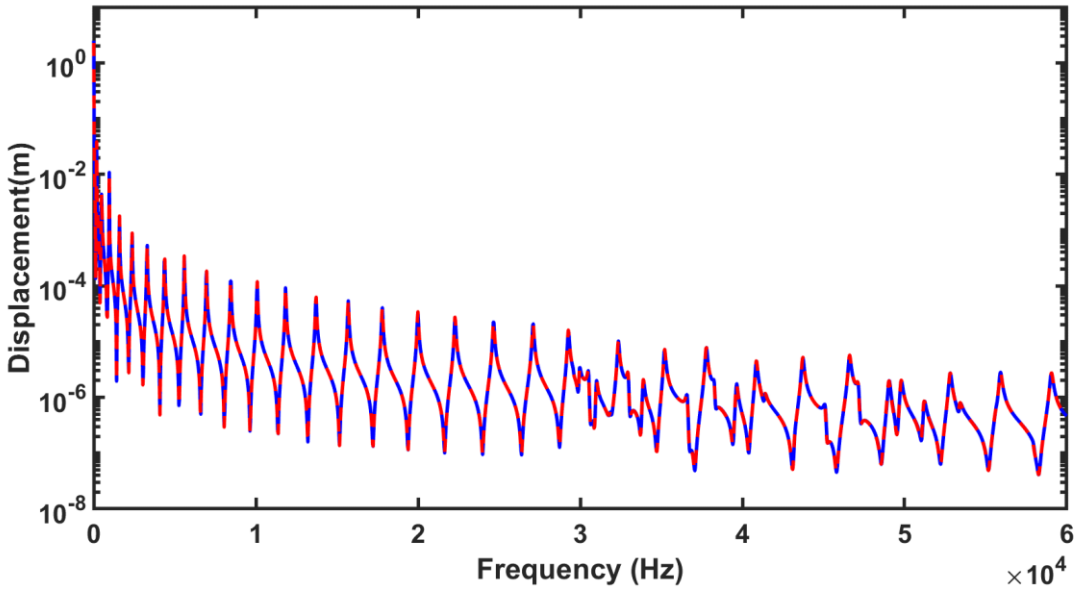

Figure 4 Forced response for $\alpha = 0.6003$ MOR (red) PMOR (blue)

4.1.3 Conclusion

The main advantage of the proposed PMOR scheme is that a reduced order model can be instantly created without having to go through the model order reduction process. There is an important possible drawback however. If completely different wave shapes are propagative for different parameters values, the global

projection basis still has to account for all of them. This may results in models several times bigger than those obtained using the simple model order reduction method. This point is important because WFEM computation time scales asymptotically with the third power of the number of degrees of freedom at the interfaces of the model. For PMOR to be a valid strategy, the increase in time computation must not offset the time required to reduce the model. Strategies are being developed to tackle this issue.

4.2 Example 2 : 3D modeling of damages in a pipe

In this section we consider a steel pipe with an inner radius of 194 millimeters and an outer radius of 203 millimeters similar to the experimental test set up in [16]. Effects of a 3D defect in the pipe are studied and analyzed using the WFEM framework in conjunction with the reduced order modeling strategies described in the previous sections. The global study strategy used is similar to that presented in [17] and the aim is medium to long range defect detection at low frequency.

4.2.1 Modeling of the cross-section

Modeling of the cross-section of the pipe was realized with ANSYS APDL 17. SOLID185 elements were used with an axisymmetric mesh with 4 elements in the wall thickness and 580 in the circumference. The elements are approximately cubic with side length of 2.25 millimeters. The model has 17400 dofs all located at its interfaces.

To model damping, we introduce a damping matrix C proportional to the stiffness matrix K. This is an elementary model which is causal and approximate hysteretic damping well when a narrow frequency band is considered. Both points are important modeling concerns when going form frequency to time domain.

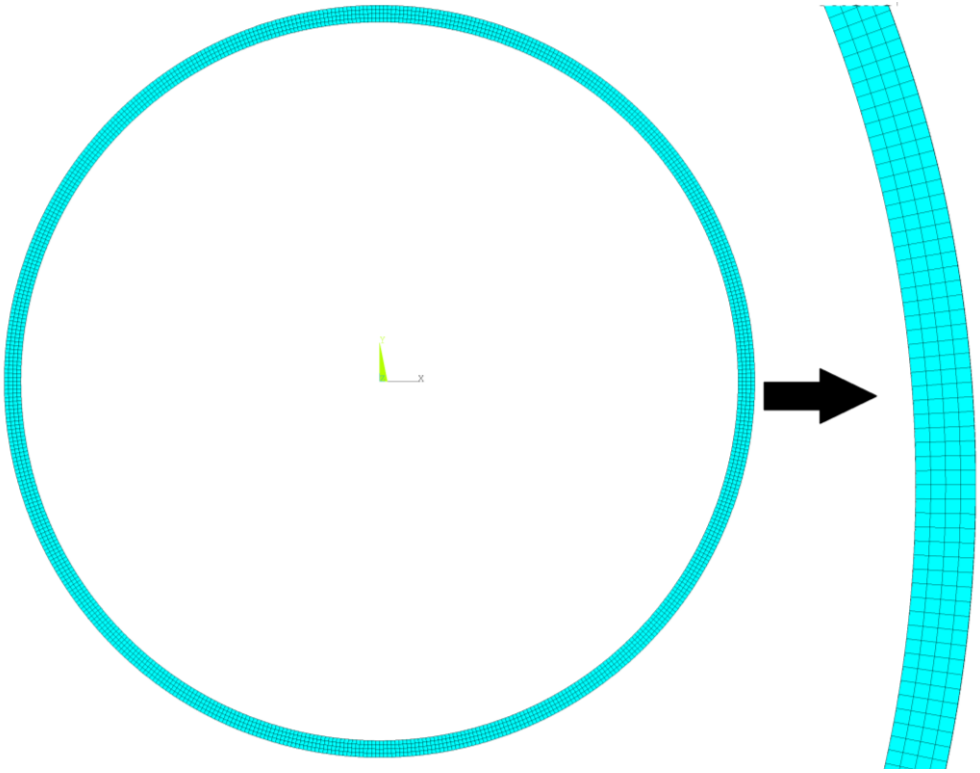

Figure 5: Mesh of the cross-section model

The material properties used are :

- Young Modulus : 210 GPa

- Poisson ratio : 0.3
- Density : 7850 $kg.m^{-3}$
- Damping stiffness ratio : $\eta_k = 10^{-3}$
- Damping stiffness frequency : $f_k = 6000\ Hz$

The damping matrix is thus given by :

$$C = \frac{\eta_k}{2\pi f_k} K \tag{18}$$

4.2.2 Modeling of the defect

We consider a defect in the cylinder in the form of a reduction of half of the wall thickness over angle θ of $\frac{\pi}{10}\ rad$ and a length of 4.5 cm. Undamaged sections are added at the beginning and the end of the defect as to make the coupling via the WFEM easier. An illustration of the model is provided in Figure 6.

Figure 6: Mesh of the defect

The model has 196908 dofs with 17400 at its interfaces. The damping and material properties used are identical to that of the cylinder.

4.2.3 Dispersion curves and choice of a wave mode

In order to get the dispersion curves of the pipe, the model order reduction strategy described above is used with $n_k = 2$ and $n_f = 1$ and $\epsilon = 10^{-4}$ to account for all propagative waves in the $[0\ ;\ 20kHz]$ frequency range. Table 2 briefly examines computation time differences between full and reduced order models.

	Original Model	**Reduced Model**
Degrees of Freedom	17400	516
Full eigenvalue problem resolution	NA (Estimated value of 39961s given $O(n^3)$ complexity)	1.11 s
Partial eigenvalue problem resolution	278 s	NA (Estimated value of 0.0073s given $O(n^3)$ complexity)
Model Order Reduction	NA	1030 s

Table 2 : Full and reduced order model comparison

Notably, a time factor of 250 is achieved even when comparing a full eigenvalue problem resolution for the reduced model to a partial resolution for the original model using Zhong's formulation [12]. The dispersion curves in Figure 7 are obtained using the reduced order model.

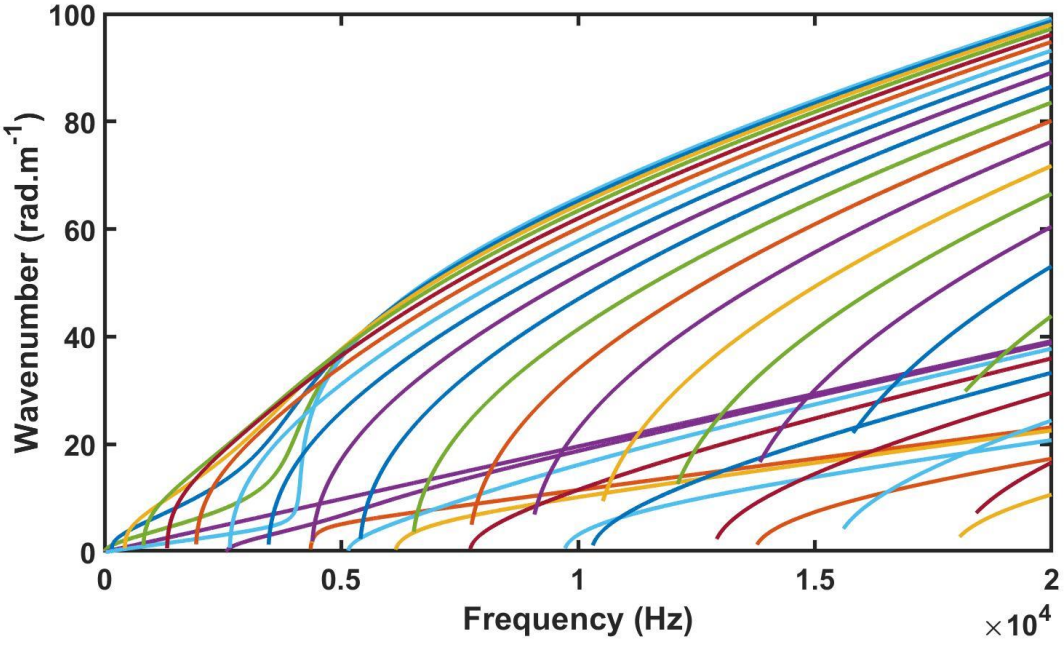

Figure 7: Dispersion curves of the pipe

We aim at detecting and if possible localizing a damaged part of the pipe at low frequency with a medium to long reach instead of at high frequency with a short reach as in [16]. Because of the respective dimensions of the pipe and defect, this means sub-wavelength detection may have to be used. In order to increase the wave-defect interactions, a high order wave mode is used as in [17] so that the circumferential size of the defect corresponds to the distance between two nodes.

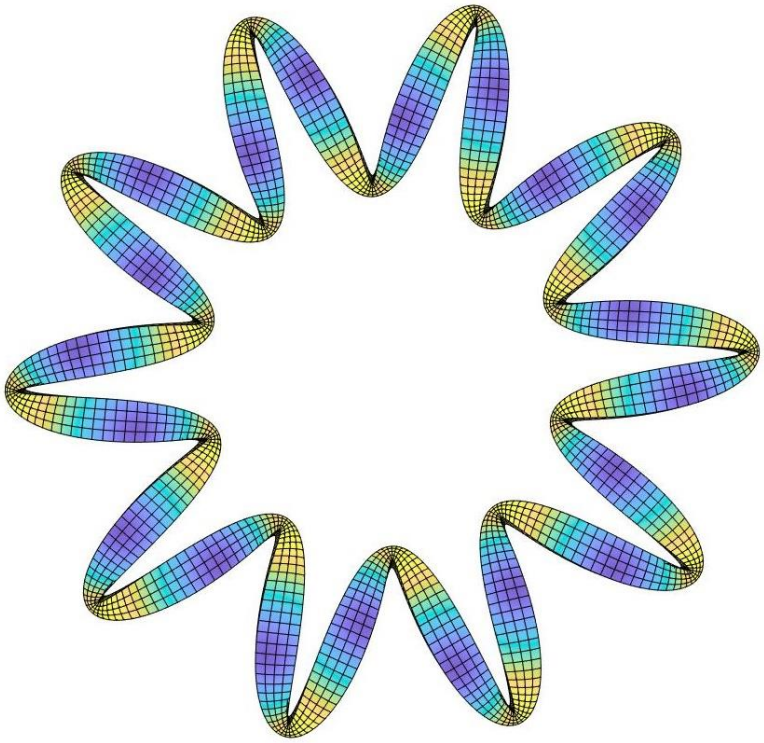

Figure 8: Chosen wave mode

The flexural mode of the 20th order (presented in Figure 8) is thus chosen for damage detection. Its cut-on frequency is slightly above $5kHz$.

4.2.4 Time domain simulations

4.2.4.1 Set up

A 36m long pipe is considered with Free-Free boundary conditions. For the simulation of the damaged pipe, the defect is located at the center of the pipe at 18m from the left end. In both cases, forces are applied on 20 points of the first cross-section to generate the 20th order flexural wave mode. The normal displacements at these points are also monitored. It is expected that the presence of the defect in the pipe leads to reflection, transmission and conversion phenomena. This can most easily be observed in time domain and is associated with a break in the spatial symmetry of the displacement field. Moreover, a premature echo due to reflection at the defect is expected. The response of the waveguide to a pulse centered at $8kHz$ is analyzed in section 4.2.4.3.

4.2.4.2 Reduced order modeling

For time domain simulations, another reduced wave basis is used for the waveguide by reducing the frequency range of interest as compared to section 4.2.3. It is obtained accounting for all propagative wave modes $[0\,;\,16kHz]$ frequency range using with parameters values $f_m = 16kHz$, $n_k = 1$, $n_f = 1$ and $\epsilon = 10^{-5}$. The reduced model of the waveguide is comprised of 524 dofs. For the defect, Craig Bampton model order reduction is used for the inner degrees of freedom. All 681 modes between 0 and 120kHz are kept. This ensures fidelity of the reduced order model without impacting computation times as the MOR process results in diagonal submatrices for the concerned dofs. The projection of the interfaces' degrees of freedom uses the same local projection basis as that of the waveguide. The model goes from 196908 to 1205 degrees of freedom. Using the WFEM framework, the frequency response functions of both waveguides are computed then time signals are obtained using a Non-uniform Discrete Fourier Transform (NDFT) with

Gaussian sampling and 8000 frequencies. The results are shown in Figure 9 and Figure 10 for a pulse of central frequency $f_c = 8000Hz$ with a Hanning window length of 100 periods. At that frequency, the group velocity of our wave mode is 930 $m.s^{-1}$. Thus, it should take 0.03871 s for a pulse to travel form one side of the pipe to the other and the same amount of time for a return trip from one end to the center of the pipe.

4.2.4.3 Time signals

Figure 9 displays the normal displacements of all 20 points of the first section multiplied by a factor $(-1)^n$ to account for the spatial symmetry of the load.

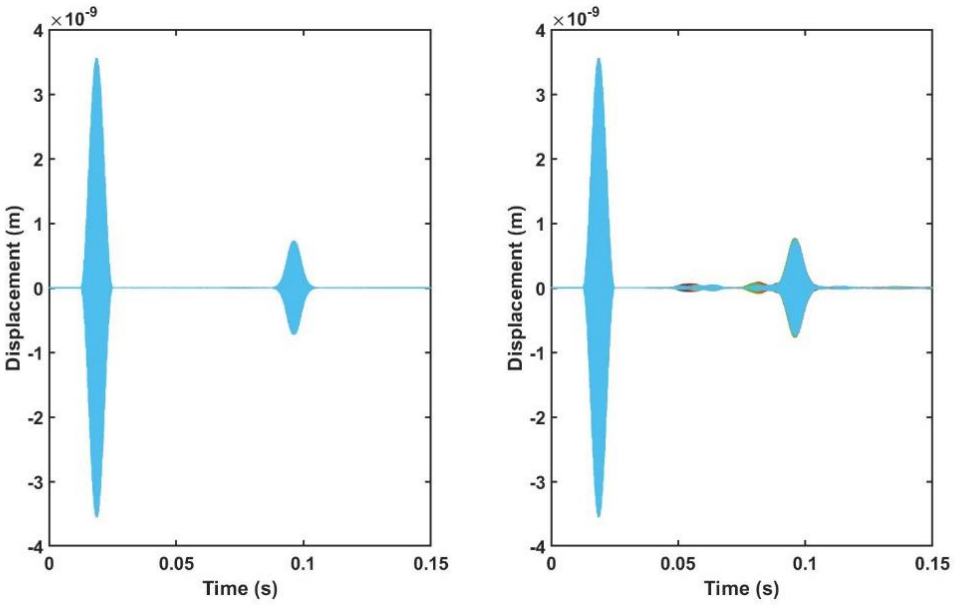

Figure 9 Time signal for all 20 points in the damaged (right) and undamaged (left) pipes

All signals are identical for the undamaged pipe but it is not the case for the damaged one. Monitoring the symmetry of the signal vector is therefore a good strategy to infer the presence of a defect. However, the asymmetric part of the vector does not allow to easily locate the defect. This is because of the conversion process in other wave modes which all have different group velocities. To solve this problem, we compute the average of all 20 signals. This is equivalent to filtering the signals to track only our wave mode since no other propagating wave shares the same symmetry. The result of this process is presented in Figure 10.

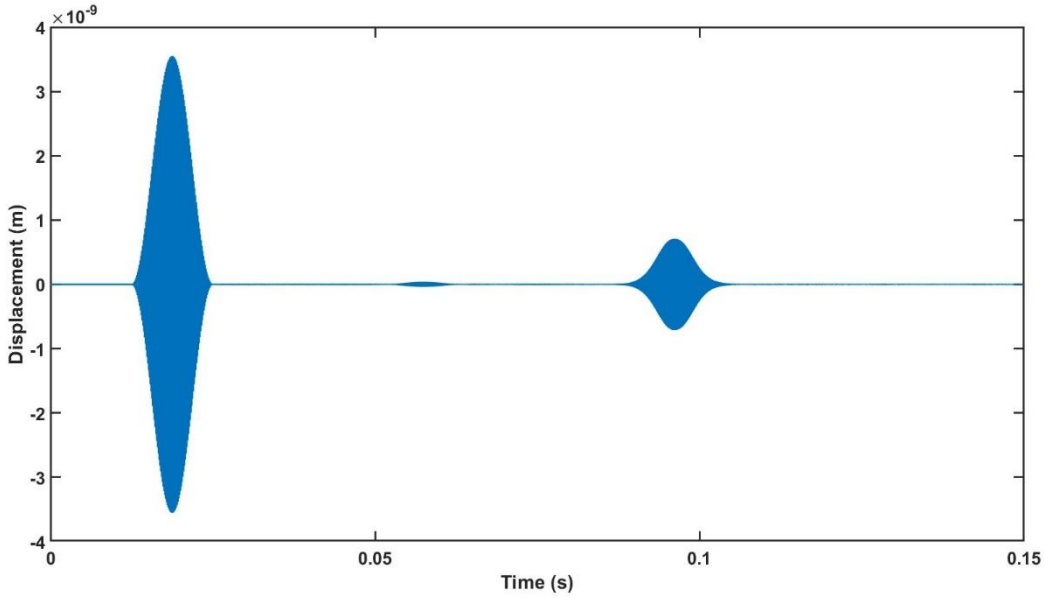

Figure 10 : average of all 20 signals in the damaged pipe

A small pulse of around 2% of the original amplitude is visible after 0.05s corresponding to wave reflection at the defect location. Indeed, the time difference between the centers of both pulses is $0.03871\ s$ which correspond to a return trip from the left end of the pipe to the defect: defect localization is achieved.

5 Conclusion

A methodology was described for reduced order modeling and parametric reduced order modeling in the WFEM framework. It was validated on a parametric sandwich model and used in the modeling of 3D wave-defect interactions in a pipe. The proposed strategy can be used to design a wave based damage-detection system by allowing fast computation of wave propagation in time domain. Lastly, some questions remain concerning the proposed PMOR scheme which will be the object of further developments.

Acknowledgements

The research of R. F. Boukadia is funded by an Early Stage Researcher grant within the European Project VIPER Marie Curie Initial Training Network (GA 675441). The research of E. Deckers is funded by a grant from the Research Foundation – Flanders (FWO). C. Claeys is a postdoctoral researcher supported through IMALIGHT. The Research Fund KU Leuven and the Flanders Make are also gratefully acknowledged for their support.

References

[1] I. Bartoli, A. Marzani, F. Lanza di Scalea and E. Viola, "Modeling wave propagation in damped waveguides of arbitrary cross-section," *Journal of Sound and Vibration*, vol. 295, pp. 685-707, 2006.

[2] U. Lee, Spectral Element Method In Structural Dynamics, Singapore: John Wiley & Sons, 2009.

[3] M. Collet, M. Ouisse and M. I. M. N. Ruzzene, "Floquet–Bloch decomposition for the computation of dispersion of two-dimensional periodic, damped mechanical systems," *International Journal of Solids and Structures,* vol. 48, pp. 2837-2848, 2011.

[4] D. J. Mead, "Vibration Response and Wave Propagation in Periodic Structures," *Transactions of the American Society of Mechanical Engineers, Journal of Engineering for Industry,* vol. 93, no. 3, pp. 783-792, 1971.

[5] J.-L. Christen, M. Ichchou, A. Zine and B. Troclet, "Wave Finite Element Formulation of the Acoustic Transmission Through Complex Infinite Plates," *Acta Acustica united with Acustica,* pp. 984-99, 2016.

[6] J. Mencik, "On the low- and mid-frequency forced response of elastic structures using wave finite elements with one-dimensional propagation," *Computers & Structures,* pp. 674-689, 2010.

[7] J. Mencik and M. Ichchou, "Multi-mode propagation and diffusion in structures through finite elements," *European Journal of Mechanics - A/Solids,* pp. 877-898, 2005.

[8] D. Duhamel, B. Mace and M. Brennan, "Finite element analysis of the vibrations of waveguides and periodic structures," *Journal of Sound and Vibration,* pp. 205-220, 2006.

[9] C. Claeys, N. G. R. de Melo Filho, L. Van Bell, E. Deckers and W. Desmet, "Design and validation of metamaterials for multiple structural stop bands in waveguides," *Extreme Mechanics Letters,* pp. 7-22, 2017.

[10] C. Zhou, J. Lainé, M. Ichchou and A. Zine, "Wave finite element method based on reduced model for one-dimensional periodic structures," *International Journal of Applied Mechanics,* 2015.

[11] C. Droz, Z. C, M. N. Ichchou and J. -P. Lainé, "A hybrid wave-mode formulation for the vibro-acoustic analysis of 2D periodic structures," *Journal of Sound and Vibration,* p. 285–302, 2016.

[12] W. X. Zhong and F. W. Williams, "On the direct solution of wave propagation for repetitive structures," *Journal of Sound and Vibration,* vol. 181, pp. 485-501, 1995.

[13] R. R. Craig and M. C. Bampton, "Coupling of substructures for dynamic analysis," *AIAA journal,* pp. 1313-1319, 1968.

[14] R. F. Boukadia, C. Droz, M. N. Ichchou and W. Desmet, "A Bloch wave reduction scheme for ultrafast band diagram and dynamic response computation in periodic structures," *Finite Elements in Analysis and Design,* 2018.

[15] P. Benner, S. Gugercin and K. Willcox, "A Survey of Projection-Based Model Reduction Methods for Parametric Dynamical Systems," *SIAM Review ,* vol. 57, no. 4, pp. 483-531, 2015.

[16] F. Schubert, B. Frankenstein, D. Hentschel, K.-J. Fröhlich, M. Küttner, B. Lamek, J. Schwenkkros and K. Kerkhof, "Structural Health Monitoring of Industrial Piping Systems Using Guided Elastic Waves," in *Deutsche Gesellschaft für Zerstörungsfreie Prüfung 2007*, 2007.

[17] C. Droz, O. Bareille, J. Lainé and M. N. Ichchou, "Wave-based SHM of sandwich structures using cross-sectional waves," *Structural Control and Health Monitoring,* vol. 25, p. e2085, 2018.